

Numerical methods to predict turbulent boundary-layer trailing edge noise for rotating blade devices

Caterina Poggi^{*1}, Giovanni Bernardini¹ and Massimo Gennaretti¹

¹Roma Tre University, Department of Civil, Computer Science and Aeronautical Technologies Engineering, Rome, Italy

^{*}*caterina.poggi@uniroma3.it*

Abstract

The proposed paper focuses on numerical methods for predicting the turbulent boundary-layer trailing edge noise in the case of rotating devices. In particular, three approaches are theoretically/numerically developed and compared: a fully analytical approach based on the Amiet theory with the inclusion of the back-scattering correction and two hybrid numerical-analytical approaches. The latter two are based on evaluating the pressure over the blades' surfaces through the Amiet model, while the noise radiation in the far field is performed numerically through the Farassat 1A formulation and its compact source version. All the approaches are successfully validated through a comparison with experimental data available in the literature. The use of numerical techniques to perform the noise radiation enhances the accuracy of the prediction even if the drawback is an increase in the required computation effort. In this framework, the exploitation of the compact-source Farassat 1A formulation, which represents the major novelty of the work, seems to be a good compromise between accuracy and computational cost.

1 Introduction

The exponential growth of city overcrowding and pollution is leading academia and industries to seek innovative and eco-friendly alternatives to standard urban transportation. In this context, Urban Air Mobility (UAM) represents a possible solution made feasible by the significant technological improvements characterizing the aviation industry, including the advances in electric propulsion and batteries. Despite the potential of this novel concept of transportation, to make UAM a viable option, some unresolved issues must be addressed, such as infrastructures, traffic management, and public acceptance in terms of environmental pollution and acoustic nuisance. Regarding this last point, the need to design low-noise vehicles is mandatory because UAM would potentially involve continuous low-altitude flyovers of cities and densely populated areas, as well as take-off and landing operations in vertiports located in urban areas. To reduce the acoustic impact of UAM on citizens, many international institutions are putting a great effort into establishing common noise regulations that prescribe maximum noise exposure levels [1]. To comply with these stringent requirements, it is of primary importance to investigate the mechanism governing the sound generation and propagation, which, due to the novelty of UAM prototypes, may be influenced by phenomena that are negligible in the standard medium-long range aviation.

Two main aspects make predicting eVTOLs aeroacoustics challenging. First, they typically operate in conditions where the rotors interact with high turbulent flows. Secondly, the limited blade tip Mach number typical of these concepts strongly increases the effect of low Reynolds number phenomena [2]. Among them, the broadband noise due to interaction between the turbulent boundary layer and the trailing edge is recognized as one of the main causes of rotor noise when operating in homogeneous stationary flows [3]. This broadband noise component is the result of the pressure fluctuations relating to the turbulent boundary layer scattered by the trailing edge [3]. Several methodologies are available in the literature to numerically predict this noise component. First, high fidelity CFD solvers [4] and LB/VLES method [5] coupled with the Ffowcs Williams and Hawkings' acoustic analogy [6] have been exploited. Alternatively, fully analytical models can be applied, such as the Amiet model [7], which directly provides the noise spectrum in the far field starting from the knowledge of the boundary-layer characteristics at the blade trailing edge. Although less accurate, they represent a numerically efficient alternative to costly high-fidelity simulations and have been widely used in the literature (see, for instance, [8]). Recently, a more accurate hybrid

analytical/numerical method has been proposed [9], which combines the Amiet model (used to determine the pressure fluctuation over the body surface) and the Farassat 1B formulation for the noise radiation. This approach has been applied also in [10], where the Amiet model has been coupled with the Farassat 1A formulation to evaluate the far-field noise.

Here, three numerical methodologies for the evaluation of the trailing edge broadband noise generated by rotating blades are applied and compared in terms of accuracy and computational cost: i) a fully analytical commonly applied formulation based on the Amiet model extended to rotating surfaces [7]; ii) a hybrid analytical-numerical method, already present in the literature [10], in which the pressure distribution over the surface of the blades is evaluated through the Amiet approach, while the noise is radiated in the far-field through the Farassat 1A formulation [11]; iii) a novel hybrid analytical-numerical method in which the noise is radiated by a compact source version of the Farassat 1A formulation [12] and the sectional fluctuating load inputs are evaluated by numerical integration of the pressure distribution over the surfaces provided by the analytical Amiet model.

This last broadband noise evaluation approach represents the major novelty of the proposed paper. The starting point is the compact source version of the Farassat 1A formulation as derived in [12] for which the sectional loads are the input data. In general, these can be considered as the superposition of a deterministic contribution, source of the tonal noise relating to the aerodynamic loads acting on the blade, and a stochastic one, relating to the trailing-edge scattering of the pressure fluctuations within the turbulent boundary layer. The deterministic contribution is determined by a quasi-steady blade element theory based on a lookup table approach which accounts for wake inflow effects. The stochastic contribution is evaluated through the Amiet airfoil self-noise model [7] extended to rotating blades through a strip-theory approach [13]. For each radial section, the stochastic pressure field is obtained by the Fourier expansion of the blade pressure waves given in [14]. This can be integrated along the blade section to obtain the sectional loads to be used as inputs in the compact-source Farassat 1A formulation.

The paper is structured as follows: first, Sec. 2 is addressed at the description of the three approaches herein applied. Then, in Sec. 3, the results of the numerical investigations are shown. In particular, the proposed methodologies are validated against literature results, and the predictions are compared in terms of accuracy and computational cost. Finally, in Sec. 4 the main outcomes of the work are summarised.

2 Boundary Layer trailing edge noise modeling

The present section addresses the theoretical/numerical description of the methodologies herein exploited, in particular, the fully analytical approach and the two hybrid numerical-analytical methods based on the combined application of the Amiet model and the Farassat 1A and its compact source version formulations.

2.1 Fully-analytical model

The analytical model herein exploited is based on the Amiet theory presented in [7] and extended in [15] to account for the effect of a finite chord length. In a right-hand system of reference centred at the midspan section trailing edge, having x_1 axis aligned with the flow direction, x_3 axis perpendicular to the trailing edge and the x_2 axis and positive on the suction side of the wing, the far-field noise Power Spectral Density (PSD) is given by [7]:

$$S_{pp}(\mathbf{x}, \omega) = \left(\frac{\omega c x_3}{2\pi c_0 \sigma^2} \right)^2 \frac{L}{2} |\mathcal{L}|^2 \Phi_{pp}(\omega) l_y(\omega) \quad (1)$$

where c and L are the wing chord and span, respectively, c_0 is the speed of sound of the undisturbed medium, ω is the frequency in radians, σ is defined as $\sqrt{x_1^2 + \beta^2(x_2^2 + x_3^2)}$, with $\beta = \sqrt{1 - M^2}$, where M is the Mach number. Furthermore, l_y denotes the spanwise correlation length, \mathcal{L} the acoustic transfer function and Φ_{pp} the wall-pressure power spectral density. Concerning the former, in the present work, the approximated expression of the spanwise correlation length proposed by Corcos in [16] is used, which reads:

$$l_y(\omega) = b_c U_c / \omega \quad (2)$$

where U_c is the convection velocity and b_c is the Corcos model constant.

The acoustic transfer function \mathcal{L} is given by the sum of two contributions, \mathcal{L}_1 , given by Amiet in [7], and \mathcal{L}_2 as defined in [15] which accounts for the back-scattering correction. For the sake of clarity, their expressions are in the following reported:

$$\mathcal{L}_1 = -\frac{e^{2iC}}{iC} \left\{ (1+i)e^{-2iC} \sqrt{\frac{B}{B-C}} E^* [2(B-C)] - (1+i)E^* [2B] + 1 \right\} \quad (3)$$

$$\mathcal{L}_2 \simeq H\{[e^{4ik}(1 - (1+i)E^*[4k])]^c - e^{2iD} + i[D + \bar{K} + \mu M - k]G\} \quad (4)$$

where

$$\begin{aligned} C &= \bar{K}_1 - \mu(x_2/\sigma - M); \quad B = \alpha\bar{K} + \mu M + k; \quad \alpha = U/U_c; \quad \mu = \bar{K}_1 M/\beta^2 \\ H &= \frac{(1+i)e^{-4ik}(1 - \Theta_1^2)}{2\sqrt{\pi}(\alpha-1)\bar{K}\sqrt{B}}; \quad D = k - \mu x_2/\sigma; \quad \epsilon = \left(1 + \frac{1}{4\mu}\right)^{-\frac{1}{2}}; \quad \Theta_1 = \sqrt{\frac{\bar{K}_1 + \mu(M+1)}{\bar{K} + \mu(M+1)}} \\ G &= (1+\epsilon)e^{i(2\bar{\mu}+D)}\frac{\sin(D-2\bar{\mu})}{D-2\bar{\mu}} + (1-\epsilon)e^{i(-2\bar{\mu}+D)}\frac{\sin(D+\bar{\mu}k)}{D+\bar{\mu}k} + \frac{(1+\epsilon)(1-i)}{2(D-2\bar{\mu})}e^{4i\bar{\mu}}E^*[4\bar{\mu}] \\ &\quad - \frac{(1-\epsilon)(1+i)}{2(D+2\bar{\mu})}e^{-4i\bar{\mu}}E^*[4\bar{\mu}] + \frac{e^{2iD}}{2}\sqrt{\frac{2\bar{\mu}}{D}}E^*[2D]\left[\frac{(1-\epsilon)(1+i)}{D+2\bar{\mu}} - \frac{(1+\epsilon)(1-i)}{D-2\bar{\mu}}\right] \end{aligned}$$

where the symbol E^* denotes the Fresnel integrals, $\bar{K}_1 = \omega/U_c$ and $\bar{\mu}$ is the acoustic wavenumber, defined as $\bar{\mu} = \bar{K}_1 M/\beta^2$.

For the evaluation of the wall-pressure power spectral density, several empirical models are available in the literature, such as the Willmarth and Roos model [17] and the Goody model [18]. In the present work, a modified version of the Goody model, proposed by Rozenberg in [19], is applied, which accounts for the adverse pressure gradient. It reads:

$$\Phi_{pp}\left(\frac{\omega\delta^*}{U_e}\right) = \frac{(\tau_w^2\delta^*/U_e)0.78(1.8\Pi\beta_c + 6)(\omega\delta^*/U_e)^2}{\left[(\omega\delta^*/U_e)^{0.75} + 0.105\right]^{3.7} + \left[3.76Re_T^{-0.57}(\omega\delta^*/U_e)\right]^7} \quad (5)$$

where U_e is the boundary layer edge velocity, δ^* the boundary layer displacement thickness, τ_w the wall shear stress, β_c is the Clauser's pressure gradient parameter. In addition, Π the wake law parameter which can be derived from the solution of the equation $2\Pi - \ln(1 + \Pi) = \kappa U_e/v_\tau - \ln(\delta^*U_e/\nu) - 5.1\kappa - \ln\kappa$, with v_τ denoting the friction velocity, ν the kinematic viscosity and κ the von Karman constant, equal to 0.41. The symbol Re_T denotes the friction Reynolds number, and it is defined as $Re_T = v_\tau\delta\sqrt{c_f}/2\nu$, where c_f is the friction velocity coefficient and δ is the boundary layer thickness.

The original Amiet model, namely Eq. (1) is valid for translating wings. Its extension to the case of rotating surfaces has been derived in [13]. In particular, following a strip theory approach, each blade is split in N strips and, for each time instant, the spectrum of the noise radiated by each blade segment is given by Eq. (1). Thus, Eq. (1) has to be intended as an instantaneous spectrum and the final PSD is obtained by summing the contributions of each segment and each blade and averaging around the azimuth angle. The assumption at the base of this approach is that the motion of each segment can be assimilated into a translating motion in the direction locally tangent to the section chord. Thus, for each azimuthal position of the blade segment, Eq. (1) can be applied. Due to this hypothesis, the relative motion between the source and the observer is neglected, and it is thereafter included through a Doppler factor correction, which reads [13]:

$$\frac{\omega}{\omega_e(\Psi)} = 1 + \frac{\mathbf{M}_t \cdot \mathbf{r}}{1 - \mathbf{M}_r \cdot \mathbf{r}} \quad (6)$$

where \mathbf{M}_t and \mathbf{M}_r represent the Mach number of the source relative to the observer and to the fluid, respectively, while \mathbf{r} represents the unit vector from the retarded source position to the observer. Furthermore, ω_e is the instantaneous emitting frequency which depends on Ψ , the blade angular position. Thus, for each blade segment, Eq. (1) is evaluated at each blade angular position Ψ and hence at each ω_e and the final spectrum is obtained by averaging over all the angular positions and weighting with the Doppler ratio in Eq. (6), namely:

$$S_{pp}(\mathbf{Y}, \omega) = \frac{N_b}{2\pi} \int_0^{2\pi} \frac{\omega_e(\Psi)}{\omega} S_{pp}^\Psi(\mathbf{x}, \omega_e) d\Psi \quad (7)$$

where S_{pp}^Ψ is the instantaneous spectrum, to be evaluated by the application of Eq. (1) at each azimuthal position Ψ , N_b is the number of blades, \mathbf{Y} denotes the coordinate of the observer in a system of reference fixed with the rotor hub while \mathbf{x} the coordinates of the observer in the (x_1, x_2, x_3) system of reference.

2.2 Hybrid analytical-numerical models

The hybrid analytical-numerical approach consists of evaluating the pressure distribution over the blade surfaces through the analytical Amiet formulation, whereas the radiation in the far field is performed numerically through the Farassat 1A formulation or its compact source version. As in the following detailed, the input data for them are, for the former formulation, the pressure distribution over the blades' surfaces, and for the latter, the section force vector associated with the pressure jump over the airfoil. Thus, the starting point for both formulations is the same: the definition of the pressure distribution over the body surfaces.

Since both the formulations do not make any assumptions about the nature of the pressure or of the associated sectional loads, they can be used to evaluate both the tonal noise at blade passing frequency harmonics and the broadband noise caused by turbulence interacting with the blade trailing edges. To this extent, the idea is to consider the pressure over the surfaces as the superposition of a deterministic contribution, source of the tonal noise and related to the aerodynamic loads acting on the blade, and a stochastic contribution, related to pressure fluctuations within the turbulent boundary-layer that are scattered as sound when they pass the trailing-edge. Focusing on the stochastic contribution, the pressure distribution is evaluated through the Amiet airfoil self-noise model [20] extended to rotating blades through a strip-theory approach [13]. Following [14], for each radial section, the stochastic pressure field is obtained by the following Fourier expansion of the blade pressure waves

$$p(\ell, \tau) = -4\pi \sum_{n=1}^N A_n \{ B_n \cos[\bar{K}_{1,n}(\ell - U_c \tau) + \phi_n] + D_n \sin[\bar{K}_{1,n}(\ell - U_c \tau) + \phi_n] \} \quad (8)$$

where N is the number of Fourier components included in the analysis (beyond which the spectrum amplitude is considered negligible), $\bar{K}_{1,n} = \omega_n/U_c$ is the n -th spanwise convective wave number and ϕ_n are independent random phase angles, distributed in $[0, 2\pi]$. In addition, in Eq. (8)

$$A_n = \left[\frac{U_c}{\pi} l_y(\omega_n) \Phi_{pp}(\omega_n, 0) \Delta k_c \right]^{1/2}, \quad B_n = e^{\epsilon \bar{K}_{1,n} y_1} - 1 + \mathcal{C}(\xi_n) + \mathcal{S}(\xi_n), \quad (9)$$

$$D_n = \mathcal{C}(\xi_n) - \mathcal{S}(\xi_n), \quad \xi_n = -y_1 [\bar{K}_{1,n} + \mu_n (1 + M)]$$

with $\mathcal{C}(\xi_n)$ and $\mathcal{S}(\xi_n)$ denoting the Fresnel cosine and sine integrals, ϵ is a positive parameter, $\mu_n = M \bar{K}_{1,n} / \beta^2$, and $\Delta k_c = \bar{K}_{1,n} / N$. The other symbols are the same already introduced in the previous section.

2.2.1 Farassat 1A formulation

In the Farassat 1A boundary integral formulation [11], the solution of the Ffowcs Williams and Hawkings equation, the acoustic pressure field is given as the superposition of the thickness noise, p'_T , depending on body geometry and kinematics,

$$4\pi p'_T(\mathbf{x}, t) = \int_{S_B} \left[\frac{\rho_0 \dot{v}_n}{r|1 - M_r|^2} \right]_{\tau} dS(\mathbf{y}) + \int_{S_B} \left[\frac{\rho_0 v_n (r \dot{\mathbf{M}} \cdot \hat{\mathbf{r}} + c_0 M_r - c_0 M^2)}{r^2 |1 - M_r|^3} \right]_{\tau} dS(\mathbf{y}) \quad (10)$$

and the loading noise, p'_L , related to the distribution of pressure over body surfaces,

$$4\pi p'_L(\mathbf{x}, t) = \frac{1}{c_0} \int_{S_B} \left[\frac{\dot{\tilde{p}} \mathbf{n} \cdot \hat{\mathbf{r}} + \tilde{p} \dot{\mathbf{n}} \cdot \hat{\mathbf{r}}}{r|1 - M_r|^2} \right]_{\tau} dS(\mathbf{y}) + \int_{S_B} \left[\frac{\tilde{p} \mathbf{n} \cdot \hat{\mathbf{r}} - \tilde{p} \mathbf{M} \cdot \mathbf{n}}{r^2 |1 - M_r|^2} \right]_{\tau} dS(\mathbf{y}) \quad (11)$$

$$+ \frac{1}{c_0} \int_{S_B} \left[\frac{\tilde{p} \mathbf{n} \cdot \hat{\mathbf{r}}}{r^2 |1 - M_r|^3} r \dot{\mathbf{M}} \cdot \hat{\mathbf{r}} \right]_{\tau} dS(\mathbf{y}) + \int_{S_B} \left[\frac{\tilde{p} \mathbf{n} \cdot \hat{\mathbf{r}}}{r^2 |1 - M_r|^3} (M_r - M^2) \right]_{\tau} dS(\mathbf{y})$$

In Eqs. (10) and (11), \mathbf{r} denotes the distance between observer position, \mathbf{x} , and source position, \mathbf{y} , whereas $\hat{\mathbf{r}} = \mathbf{r}/r$ is the unit vector along the source-observer direction, with $r = |\mathbf{r}|$. In addition, c_0 and ρ_0 are speed of sound and density in the undisturbed medium, respectively, $\tilde{p} = (p - p_0)$ with p_0 representing the undisturbed medium pressure, $\mathbf{M} = \mathbf{v}_B / c_0$ with \mathbf{v}_B denoting the body velocity, $M = \|\mathbf{M}\|$ and $M_r = \mathbf{M} \cdot \hat{\mathbf{r}}$. Further, \dot{v}_n , $\dot{\mathbf{n}}$ and $\dot{\mathbf{M}}$ denote time derivatives of v_n , \mathbf{n} and \mathbf{M} , observed in a frame of reference fixed with the undisturbed medium. Notation $[\dots]_{\tau}$ indicates that these quantities are evaluated at the emission time, $\tau = t - \theta$, where θ is the time taken by the signal started from $\mathbf{y} \in S_B$ to reach the observer at time t .

As already stated, the pressure distribution \tilde{p} is divided in a deterministic contribution and in a stochastic one. The former is evaluated through a Boundary Element Method (BEM) aerodynamic solver based on the boundary integral formulation for potential and incompressible flows [21], while the stochastic contribution is evaluated through Eq. (8).

2.2.2 Compact-source Farassat 1A formulation

Under the assumptions of negligible blade chord length with respect to the source-observer distance and limited values of chordwise pressure gradients, the compact-source version of the Farassat 1A boundary integral formulation [22] can be applied. Similarly to the Farassat 1A formulation described in the previous section the aeroacoustic pressure field is given by the superposition of the thickness and the loading noise terms. For the compact-source formulation, the latter is associated with the blade sectional loads instead of the pressure distribution over the surface. Starting from the 1A Farassat formulation, assuming a slender rotor blade, the thickness term can be expressed as a combination of line integrals along the spanwise quarter-chord line, D_s [23]:

$$4\pi p'_T(\mathbf{x}, t) = \int_{D_s} \left[\frac{A\dot{W}}{r^2|1-M_r|^4} \right]_\tau ds(\mathbf{y}) + 3 \int_{D_s} \left[\frac{AW^2}{r^3|1-M_r|^5} \right]_\tau ds(\mathbf{y}) - c_0 \int_{D_s} \left[\frac{AM_r W}{r^3|1-M_r|^4} \right]_\tau ds(\mathbf{y}) \quad (12)$$

where

$$W = r\dot{M} \cdot \hat{\mathbf{r}} + c_0(M_r - M^2)$$

where A is the blade cross-section area, s is the corresponding (curvilinear) coordinate of integration.

Similarly, the compact version of the loading contribution is given by [22]

$$4\pi p'_L(\mathbf{x}, t) = \frac{1}{c_0} \int_{D_s} \left[\frac{\dot{\mathbf{L}} \cdot \hat{\mathbf{r}}}{r|1-M_r|^2} \right]_\tau ds(\mathbf{y}) + \int_{D_s} \left[\frac{\mathbf{L} \cdot (\hat{\mathbf{r}} - \mathbf{M})}{r^2|1-M_r|^2} \right]_\tau ds(\mathbf{y}) \\ + \int_{D_s} \left[\frac{\mathbf{L} \cdot \hat{\mathbf{r}}}{r^2|1-M_r|^3} \left(\frac{r\dot{M} \cdot \hat{\mathbf{r}}}{c_0} + M_r - M^2 \right) \right]_\tau ds(\mathbf{y}) \quad (13)$$

where,

$$\mathbf{L} = - \int_{D_c} \Delta p \mathbf{n} d\ell \quad (14)$$

is the section force vector, where D_c is the chordwise domain of integration, ℓ is the corresponding (curvilinear) coordinate of integration, whereas \mathbf{n} and Δp denote upward unit-normal to airfoil mean-line and pressure jump, respectively. Following the approach above described, the section force vector, \mathbf{L} , is conceived as the sum of the section aerodynamic loads associated with the deterministic pressure jump, \mathbf{L}_d , and the stochastic ones \mathbf{L}_s (i.e., $\mathbf{L} = \mathbf{L}_d + \mathbf{L}_s$). The deterministic section airloads, \mathbf{L}_d , are determined by a quasi-steady blade element theory based on a lookup table approach, which accounts for wake inflow effects [24]. The stochastic contribution, \mathbf{L}_s , is evaluated through the Amiet airfoil self-noise model [20]. In particular, starting from the expression of the pressure distribution over the surface, namely Eq. (8), observing that the random phase angles are independent on the chordwise coordinate, substituting Eq. (8) in Eq. (14), the following expression of the sectional loads associated with the stochastic pressure jump is obtained:

$$\mathbf{L}_s = \sum_{n=1}^N A_n [\mathbf{L}_{s,n}^c \cos(\phi_n - U_c \tau) + \mathbf{L}_{s,n}^s \sin(\phi_n - U_c \tau)] \quad (15)$$

where

$$\mathbf{L}_{s,n}^c = 4\pi \int_{D_c} (B_n \cos(\bar{K}_{1,n} \ell) + D_n \sin(\bar{K}_{1,n} \ell)) \mathbf{n} d\ell \\ \mathbf{L}_{s,n}^s = 4\pi \int_{D_c} (-B_n \sin(\bar{K}_{1,n} \ell) + D_n \cos(\bar{K}_{1,n} \ell)) \mathbf{n} d\ell \quad (16)$$

Eq. (16) can be integrated numerically to obtain the sectional loads to be given as input to Eq. (13).

It is important to highlight that for the compact-source formulation, the pressure distribution in Eq. (8) has to be intended as the pressure over the chord mean line. Thus, when the integration of Eq. (16) is performed, the pressure of Eq. (8) is split half on the suction side and half on the pressure side of the airfoil.

3 Numerical results

The proposed approaches are validated through a comparison with the literature results presented in [8]. The test case consists of a two-bladed fan in hovering condition, having a radius equal to 400 mm and a rotational speed of 600 rpm. For other details about the configuration, the reader is referred to [8]. The results are shown in terms of Power Spectral Density (PSD) evaluated assuming the reference pressure equal to $2 \cdot 10^{-5}$ Pa. Furthermore, only the broadband trailing edge noise contribution is investigated. In particular, in a right-hand system of reference with origin in the rotor hub, z-axis coincident with the rotational axis, y-axis directed radially and pointing starboard, the microphone is located at (1.09 m, 0 m, 1.30 m).

First, the fully analytical method (described in Sec. 2.1) is applied. The blade is divided into 7 strips, where the geometrical characteristics are known, as described in [8] and reported in Tab. 1 for the sake of clarity.

	Strip # 1	Strip # 2	Strip # 3	Strip # 4	Strip # 5	Strip # 6	Strip # 7
Radius, r [m]	0.155	0.195	0.235	0.275	0.315	0.355	0.395
Chord, c [m]	0.12	0.12	0.125	0.13	0.13	0.135	0.135
Stagger angle, γ [deg]	47.8	49.7	51.9	53.8	55.6	57.7	59

Table 1: Geometrical data of the blade [8].

To evaluate the trailing edge noise by applying Eq. (1), first, the wall-pressure PSD has to be evaluated. In this framework, two different approaches have been applied and compared. First, the analytical model in Eq. (5) is exploited. The standard formulation described in [25] is used to evaluate the boundary layer quantities, starting from the Reynolds number at each blade section. In particular:

$$\frac{\delta^*}{c} = \frac{0.0477}{Re_c^{1/5}} \quad c_f = \frac{0.0594}{Re_c^{1/5}} \quad \tau_w = \frac{1}{2} \rho U^2 c_f \quad (17)$$

where Re_c is the Reynolds number based on the chord and the mean velocity. In addition, the convective velocity and the Corcos constant given in [8] are used. In particular, in the section of the midspan set $U_c/U = 0.75$ and $b_c = 1.56$, whereas in the section in the blade-tip set $U_c/U = 1.07$ and $b_c = 0.9$.

The second approach applied to evaluate the wall-pressure spectrum is based on the experimental measurements reported in [8], suitably extrapolated to the section of interest by assuming the flow to be self-similar. The predictions obtained with the two approaches are shown in Fig. 1 where a comparison with the experimental and analytical results in [8] is also reported.

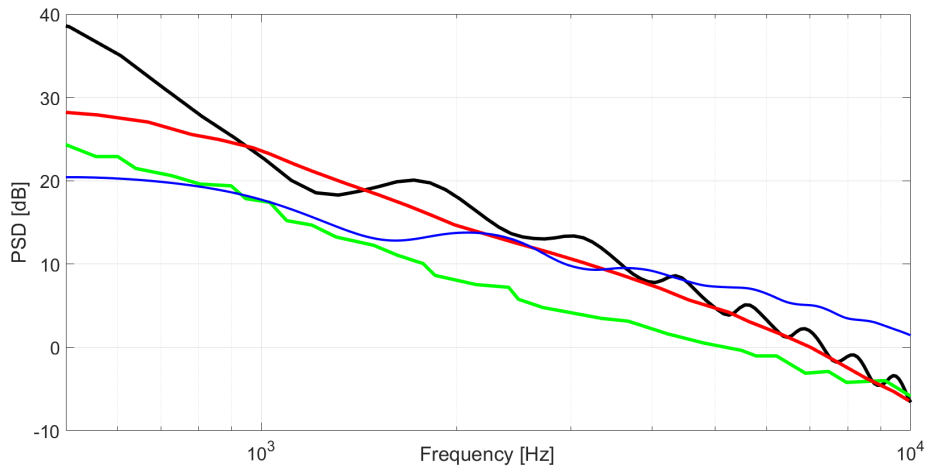


Figure 1: Comparison between the analytical model predictions (blue line with analytical wall-pressure PSD, black line with the experimental wall-pressure PSD provided in [8]) and the literature results in [8] (green line experimental data, red line analytical predictions).

This comparison shows that when the wall-pressure PSD is evaluated starting from the experimental measurements, a good agreement with the analytical prediction of [8] is obtained. Indeed, the main trend is well captured,

even if the obtained results exhibit a slightly more wavy behaviour in almost the whole range of frequencies examined and overestimate the SPL at the lowest frequency (namely $f < 10^3$) up to 10 dB. Instead, when the wall-pressure PSD is evaluated through the analytical relation in Eq. (5), the slope of the curve changes. This implies that when compared with the analytical results of [8], at the lower frequencies, the far-field PSD is underestimated, whereas the opposite occurs at the highest frequencies investigated (namely $f > 3 \cdot 10^3$). Focusing instead on the comparison with the experimental data, when the experimental wall-pressure spectra are used, an overestimation of the far-field PSD is obtained which is slightly reduced as the frequency increases. Contrarily, when the wall-pressure spectra are evaluated through the analytical expression, a better agreement is obtained at the lowest frequency, but a significant overestimation, up to 8 dB, is observed as the frequency increases. It is important to highlight that it is a well-known problem the difficulty in reliably numerically predicting the wall-pressure spectrum, as well as the boundary layer parameters for its evaluation. At the same time, their accurate estimation is fundamental for a reliable estimation of the radiated noise. Nevertheless, it is beyond the scope of the proposed research to investigate on the effect of the wall-pressure spectrum PSD. For this reason, in the following, only the results obtained from the analytical wall-pressure spectra of Eq. (5), with the boundary layer quantities estimated through the relation in [25], are used.

Then, the two hybrid analytical/numerical methodologies have been applied. The Farassat 1A formulation (described in Sec. 2.2.1) is applied considering a blade surface discretization with 50 elements along the chord and 30 along the radius. The compact-source Farassat 1A formulation (detailed in Sec. 2.2.2) is applied considering the blade discretized in 30 sections. Furthermore, 50 elements are considered along the chord to numerically integrate the pressure distribution and obtain the sectional forces vector, namely to solve Eq. (14). As verified through a preliminary convergence analysis, these discretizations are sufficient to guarantee solutions that are not affected by further mesh refinements. For the time discretization, a $\Delta t = 0.00005s$ is used for both formulations, whereas the acquisition period is one rotor revolution.

Figure 2 shows the predictions obtained through the hybrid method based on the noise radiation through the Farassat 1A formulation and the novel approach based on the compact-source formulation, compared with the experimental data presented in [8] and the predictions obtained through the fully analytical method, namely Eq. (1). Note that the predictions through the hybrid approaches have been obtained by averaging five stochastic samples, namely five different random generator seeds in the evaluation of the surface pressure, namely Eq. (8).

Overall, the results obtained through the novel approach are satisfactory and comparable to those obtained from the other numerical approaches considered. In particular, the results obtained through the two hybrid numerical-analytical approaches are in quite good agreement, mainly for frequencies higher than 10^3 . Indeed, at lower frequencies, the compact Farassat 1A provides a PSD which is about 4 dB lower than the predictions obtained through the non-compact Farassat 1A. Comparing the hybrid numerical-analytical approaches results with the fully-analytical one, we observe that the former predict higher SPLs for frequencies lower than $2 \cdot 10^3$, and lower SPLs for frequencies higher than $5 \cdot 10^3$. Compared with the experimental data, an overestimation of about 6 dB is observed in almost the whole frequency range considered, which slightly decreases as the frequency increases.

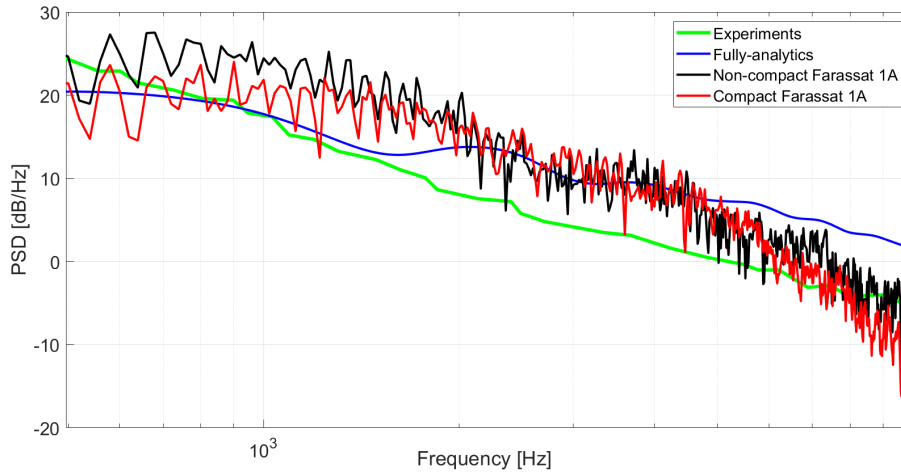


Figure 2: Comparison between the numerical models and the experimental results in [8]

As already highlighted, the differences between the experiments are probably due to the uncertainties in evaluating the boundary-layer parameters and the low accuracy of the analytical models used to evaluate the wall pressure spectra inputs.

4 Conclusion

Three different numerical approaches for the evaluation of the broadband trailing edge noise have been proposed and compared: a fully analytical approach based on the Amiet theory, widely used in the literature, and two hybrid numerical-analytical approaches based on the combination of the Amiet theory for the evaluation of the pressure field over the propeller blades with the numerical radiation in the far-field based on the Farassat 1A formulation or its compact source version. The latter represents the major novelty of the work. All the approaches have been validated through a comparison against literature results and experimental data. The level of accuracy of all the aforementioned approaches is satisfactory. In particular, focusing on the fully analytical approach, when the experimental wall pressure spectra are used, the outcomes are in very good agreement with the literature results. Instead, if analytical models are used, some discrepancies arise. In particular, a change in the spectrum slope is observed, resulting in an underestimation at the lower frequencies and an overestimation at higher ones. Focusing on the hybrid analytical-numerical approaches, they provide similar results, mainly at frequencies higher than 10^3 and in agreement with those provided by the fully analytical approach. The major difference resides in the computational cost. Indeed, the fully analytical model is the fastest one, whereas the hybrid approaches require a greater computational effort. Using the compact source Farassat 1A reduces the computational time by about a fifth with respect to the non-compact Farassat 1A. Since the outcomes are in very good agreement, the novel methodology seems suitable for predicting the radiated noise.

References

- [1] I. C. A. Organization, "Guidance on the balanced approach to aircraft noise management," tech. rep., ICAO, 2008.
- [2] S. A. Rizzi *et al.*, "Urban air mobility noise: Current practice, gaps, and recommendations," tech. rep., 2020.
- [3] T. F. Brooks, D. S. Pope, and M. A. Marcolini, "Airfoil self-noise and prediction," tech. rep., 1989.
- [4] C. Wagner, T. Hüttl, and P. Sagaut, *Large-eddy simulation for acoustics*, vol. 20. Cambridge University Press, 2007.
- [5] K. Kusano, K. Yamada, and M. Furukawa, "Aeroacoustic simulation of broadband sound generated from low-mach-number flows using a lattice boltzmann method," *Journal of Sound and Vibration*, vol. 467, p. 115044, 2020.
- [6] H. D. Ffowcs Williams, JE, "Sound generated by turbulence and surfaces in arbitrary motion," *Philosophical Transactions of the Royal Society*, p. A264, 1969.
- [7] R. K. Amiet, "Noise due to turbulent flow past a trailing edge," *Journal of sound and vibration*, vol. 47, no. 3, pp. 387–393, 1976.
- [8] Y. Rozenberg, M. Roger, and S. Moreau, "Rotating blade trailing-edge noise: Experimental validation of analytical model," *AIAA journal*, vol. 48, no. 5, pp. 951–962, 2010.
- [9] J. Casper and F. Farassat, "Broadband noise predictions based on a new aeroacoustic formulation," in *40th AIAA Aerospace Sciences Meeting & Exhibit*, p. 802, 2002.
- [10] M. Barbarino and D. Casalino, "Hybrid analytical/numerical prediction of propeller broadband noise in the time domain," *International Journal of Aeroacoustics*, vol. 11, no. 2, pp. 157–175, 2012.
- [11] F. Farassat, "Derivation of formulations 1 and 1a of farassat," 2007.
- [12] G. Bernardini, M. Gennaretti, and C. Testa, "Spectral-boundary-integral compact-source formulation for aero-hydroacoustics of rotors," *AIAA Journal*, vol. 54, no. 11, pp. 3349–3360, 2016.
- [13] R. Schlinker and R. Amiet, "Helicopter rotor trailing edge noise," in *7th Aeroacoustics Conference*, 1981.

- [14] J. Casper and F. Farassat, "Broadband trailing edge noise predictions in the time domain," *Journal of Sound and Vibration*, vol. 271, no. 1-2, pp. 159–176, 2004.
- [15] M. Roger and S. Moreau, "Back-scattering correction and further extensions of amiet's trailing-edge noise model. part 1: theory," *Journal of Sound and vibration*, vol. 286, no. 3, pp. 477–506, 2005.
- [16] G. Corcos, "The structure of the turbulent pressure field in boundary-layer flows," *Journal of Fluid Mechanics*, vol. 18, no. 3, pp. 353–378, 1964.
- [17] W. Willmarth and F. Roos, "Resolution and structure of the wall pressure field beneath a turbulent boundary layer," *Journal of Fluid Mechanics*, vol. 22, no. 1, pp. 81–94, 1965.
- [18] M. Goody, "Empirical spectral model of surface pressure fluctuations," *AIAA journal*, vol. 42, no. 9, pp. 1788–1794, 2004.
- [19] Y. Rozenberg, *Modélisation analytique du bruit aérodynamique à large bande des machines tournantes: utilisation de calculs moyennés de mécanique des fluides*. PhD thesis, Ecole Centrale de Lyon, 2007.
- [20] R. K. Amiet, "High frequency thin-airfoil theory for subsonic flow," *AIAA journal*, vol. 14, no. 8, pp. 1076–1082, 1976.
- [21] M. Gennaretti and G. Bernardini, "Novel boundary integral formulation for blade-vortex interaction aerodynamics of helicopter rotors," *AIAA journal*, vol. 45, no. 6, pp. 1169–1176, 2007.
- [22] B. Kenneth S and J. Henry E, "Noise prediction for maneuvering rotorcraft," 2000.
- [23] L. V. Lopes, "Compact assumption applied to monopole term of farassat's formulations," *Journal of Aircraft*, vol. 54, no. 5, pp. 1649–1663, 2017.
- [24] W. Johnson, *Rotorcraft aeromechanics*, vol. 36. Cambridge University Press, 2013.
- [25] H. Schlichting and J. Kestin, *Boundary layer theory*, vol. 121. Springer, 1961.